J Mater Sci (2010) 45:3088–3095
DOI 10.1007/s10853-010-4316-8

Experimental observation and computer simulation of conic markings on fracture surfaces of polymers

Peihua Du · Bin Xue · Yihu Song · Min Zuo · Shengjun Lu · Qiang Zheng · Jie Yu

Received: 27 October 2009 / Accepted: 10 February 2010 / Published online: 2 March 2010

Abstract The morphology of conic markings was observed on the fracture surfaces of amorphous polysulfone, polyethersulfone and polyetherimide and semicrystalline polypropylene, polyphenylene sulfide and polybutylene terephthalate by using scanning electron microscopy. Most of conics exhibit the stepped stereo configuration, and the origin of secondary crack is depressed in the crack plane as a result of plastic deformation. The brittle–ductile transition of polymers can be analyzed by comparing the matching morphology of conic markings. According to computer simulations, the type I marking is determined by the ratio of the main to the secondary crack velocity while the type II marking is determined by the distances that two secondary cracks have covered before they meet. Variations of conic shapes can help to determine the changes of crack growth velocity.

Introduction

Fracture surfaces of polymers can exhibit certain characteristic patterns recording the fracture process. In general, common patterns include conic markings, radial striations, regularly spaced rib markings, periodic bands, etc. [1]. An examination of these patterns provides valuable information involved in the failure mechanisms [2–11].

P. Du · Y. Song · M. Zuo · Q. Zheng (✉)
Department of Polymer Science and Engineering, Zhejiang University, Hang Zhou 310027, China
e-mail: zhengqiang@zju.edu.cn; zhengqiang@zjuem.zju.edu.cn

P. Du · B. Xue · Y. Song · S. Lu · Q. Zheng · J. Yu
National Engineering Research Center for Compounding and Modification of Polymeric Materials, Guiyang 550014, China

Conic marking is a kind of important pattern on fracture surfaces. It is generally accepted that the conic marking forms due to the intersection between a moving main planar crack front and a radically growing circular craze or secondary crack front [9, 12–17]. The nucleation, growth, and coalescence of cracks in the formation of conic marking determine the micromechanism of dynamic fracture [14].

Conic marking has been observed in amorphous polymers such as poly(methyl methacrylate) (PMMA) [13–15] and epoxy [12, 17] while it has rarely been observed in semicrystalline polymers. Moreover, very little attention has been paid to the stereo configuration of the two matching fracture surfaces.

Computer simulation has been used to study the fracture patterns [9, 12, 17–21]. It is reported that the conic marking can change from a parabola or a prolate parabola to an ellipse, and finally to an approximate circle as the velocity ratio of the main crack to the secondary crack increases [9, 12]. The previous simulations could hardly disclose all the forming mechanism of conic markings, especially the type II markings formed by intersection of two radial growing secondary cracks. The previous simulation results did not have experimental support.

In the present research, we observe the conic markings on the fracture surfaces of a wide range of polymers including amorphous polysulfone (PSF), polyethersulfone (PES), and polyetherimide (PEI) as well as semicrystalline polypropylene (PP), polyphenylene sulfide (PPS), and polybutylene terephthalate (PBT). We analyze the nucleation of secondary crack and the stereo morphology of conic markings on the matching surfaces. The formation mechanism and influencing factors for the formation of conic markings are investigated by a combination of scanning electron microscopy (SEM) observations and computer simulation.

Experimental procedure

The resins used were PSF (Solvay, P-3500, Brussels, Belgium), PES (Sumitomo, 4100G, Kobe, Japan), PEI (G.E, 1000, Connecticut, USA), PP (Olefin Plant in Liaoyang Petrochem. Co., 4016, Liaoyang, China), PPS (Polyplastics, HS-G30, Chiba, Japan), and PBT (Jiangsu Yizheng Chem. Fiber Co., S3130, Yizheng, China), respectively. All the specimens were made by injection molding and dimensions are provided in Scheme 1 of Fig. 1.

Tensile tests were carried out on a universal testing machine (WdW-10C, Hualong Testing Instruments Co. Ltd., Shanghai, China) according to GB1040-92 in a loading velocity range of 0.1–1000 mm/min at room temperature. Impact tests were conducted on a pendulum impact testing machine (ZBC-4B, Shenzhen Xinsansi Measurement Equipment Co., Shenzhen, China) according to GB/T1843-1996 at temperatures from −196 to 180 °C. The three-point bending tests were performed on the universal testing machine in a loading velocity ranging from 0.05 to 500 mm/min.

The fracture surfaces of the specimens after being coated with gold were observed using a scanning electron microscope (SEM, KYKY-2800B, Kyky Co., Beijing, China). Atomic force microscope (AFM, SPI3800N, Seiko Instruments Inc., Tokyo, Japan) was used in the tapping model to observe the stereo configuration of conic marking.

Results and discussion

Morphology observation of conic markings

Formation of conic markings

Figure 1 gives the type I and type II conic markings observed through SEM and the illustration of formation mechanism of conic marking. Each conic marking contains a secondary initiation at the focus. Conic markings are produced not only by the intersection of a main crack front with a secondary crack (type I), but also by the interaction of one secondary crack with another (type II).

The forming of conic marking needs several conditions [13, 22]. Figure 2 shows the morphology of secondary initiation within conic markings. Defects or inhomogeneities (Fig. 2a), microvoids (Fig. 2b), and even spherulites (Fig. 2c, d) in semicrystalline polymers may be the

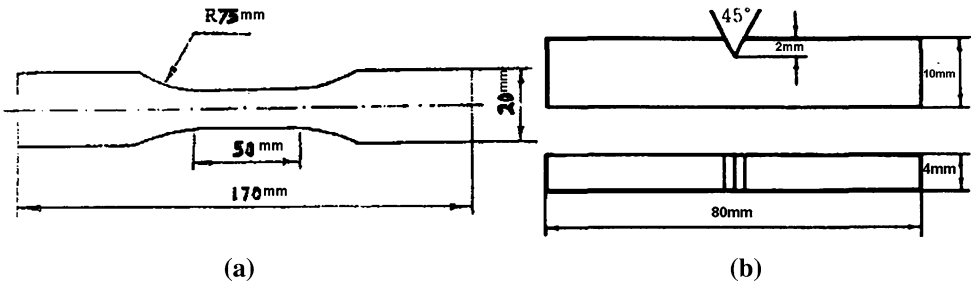

Scheme 1 Illustrations of dimensions of specimen used in tensile (**a**) and in impact and bending tests (**b**)

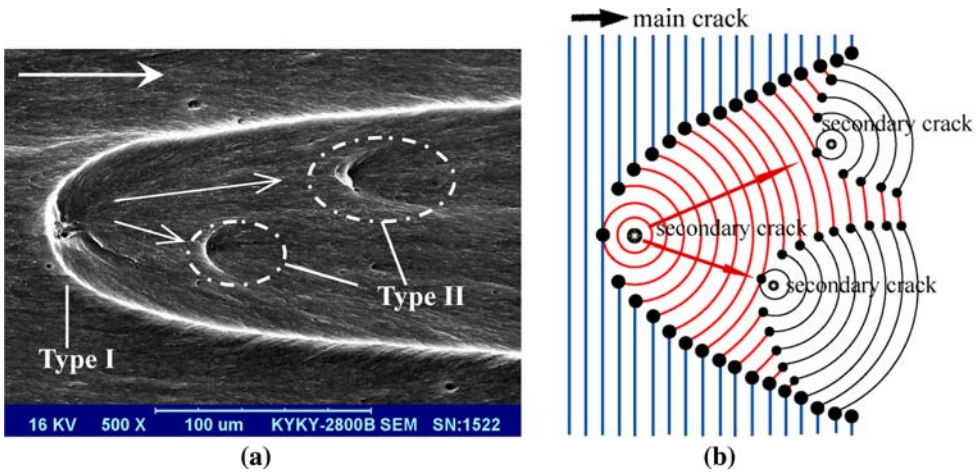

Fig. 1 **a** SEM micrograph of conic markings on the bending fracture surface of PPS tested at 190 mm/min. The *white arrows* denote the direction of crack propagation. **b** Schematic diagram for the formation mechanism of conic markings

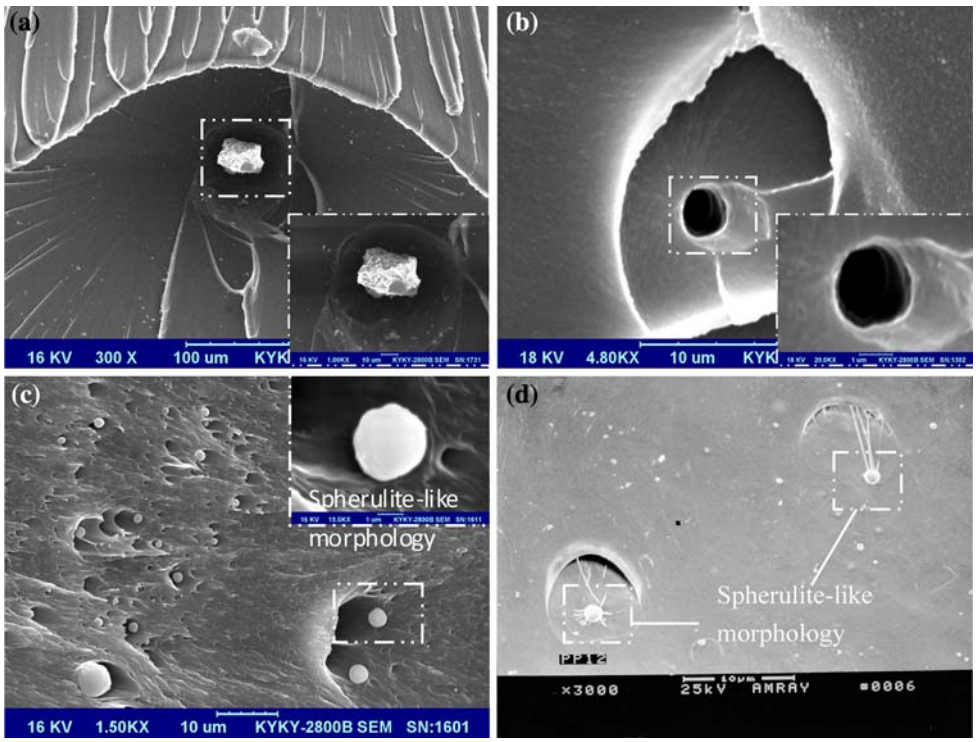

Fig. 2 SEM micrographs showing secondary initiation within conic markings: **a** impurity on tensile fracture surface of PSF tested at 1 mm/min, **b** microvoid on tensile fracture surface of PSF tested at 1 mm/min, **c** spherulite-like morphology on bending fracture surface of PPS tested at 500 mm/min, and **d** spherulite-like morphology on tensile fracture surface of PP tested at 20 mm/min

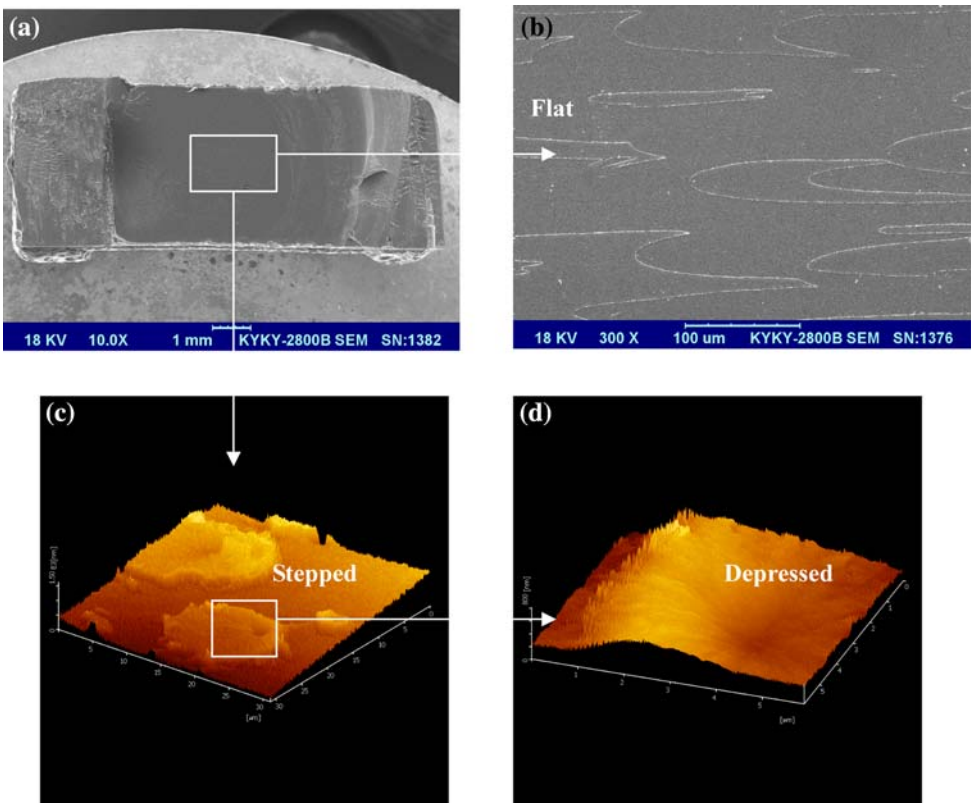

Fig. 3 Stereo observations of conic marking on fracture surfaces of PSF tested at 140 °C: **a** SEM micrograph of the whole impact fracture surface, **b** magnified SEM micrograph of conic markings, **c** AFM micrograph of the conic markings, and **d** AFM micrograph of the depressed secondary crack initiation

potential sources for initiating the secondary cracks. Injection moldings usually yield complex microstructural distributions in amorphous and semicrystalline polymers [23–40]. The complex changes and especially discontinuities in preferred orientation and residual stresses and density distributions should play a role in the crack

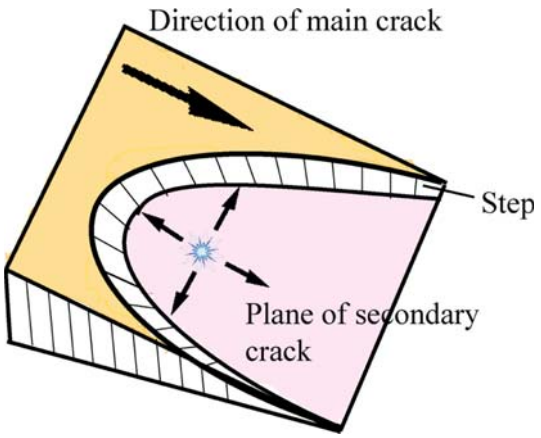

Fig. 4 Schematic diagram for the formation of a step at the junction between a main and a secondary crack

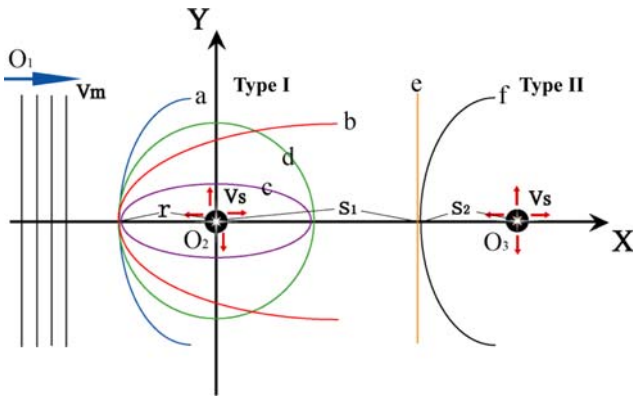

Fig. 6 Schematic diagram for cracks and conic markings in reference to the coordinate systems. Curves *a*, *b*, *c*, and *d* denote the type I conic markings with increasing V_m/V_s gradually. Curves *e* and *f* denote the type II conic markings for $S_1 = S_2$ and $S_1 \neq S_2$

propagation [35–40]. In the case of spherulitic morphologies [41], the relatively high-residual stresses and anisotropy facilitate spherulites to easily break away from the matrix under external loads and to trigger the formation of secondary cracks.

Stereo morphology of conic markings

Among the SEM micrographs of the fracture surfaces of the six polymers, the conic markings on the impact fracture surface of PSF are the most flat. Figure 3 shows the stereo morphology of conic marking on impact fracture surfaces of PSF tested at 140 °C. Even the rather flat conic shapes observed under SEM (Fig. 3a, b) still exhibit stepped shapes under AFM (Fig. 3c). In fact, most conic markings are stepped in stereo space.

The flaws are naturally and randomly dispersed throughout the material [14] so that the nuclei of secondary fracture are usually not on the same plane as the main cracks. The fronts of these two cracks intersect in space, leaving a level difference boundary on the fracture surface. Figure 4 shows the space interaction of the two fracture fronts and the focus of the conic identifying the origin of the secondary fracture front.

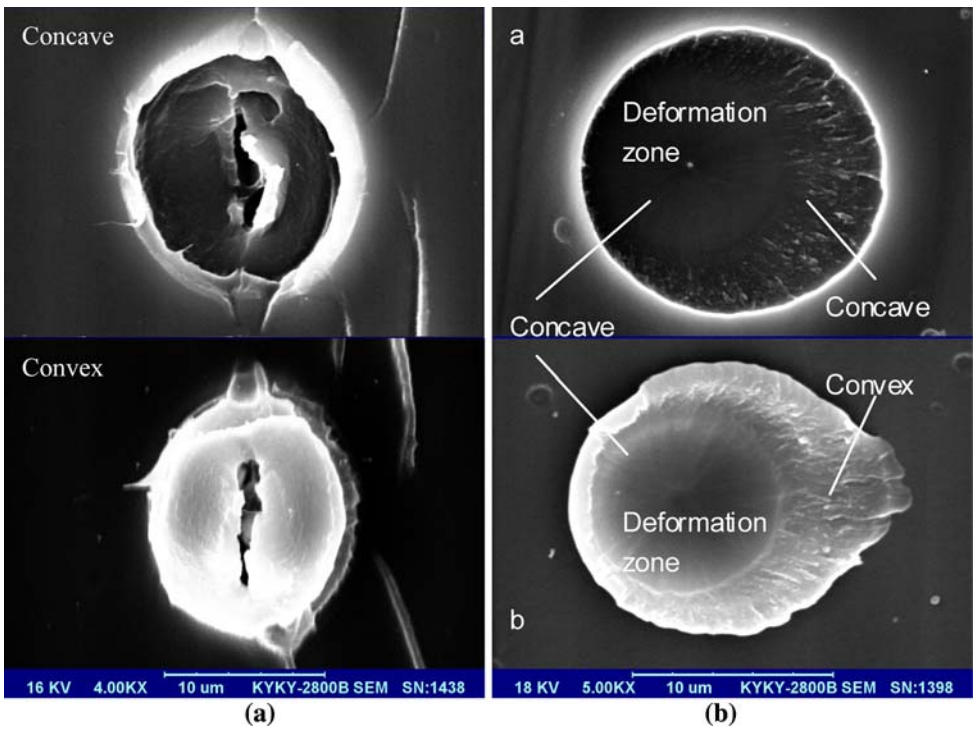

Fig. 5 SEM micrographs of conic marking morphology on the two matching bending fracture surfaces of PES tested at **a** 50 mm/min and **b** 0.05 mm/min

Using AFM, we could observe that the secondary crack origin is depressed in the plane of secondary crack (Fig. 3d). The degree of plastic deformation determines the matching condition between the two matching fracture surfaces. The deformation zone, which is the slow growth area of the secondary crack, usually appears concave on both surfaces, while the fast growth zone in the secondary crack would appear concave on one surface and convex on its mating surface.

Figure 5 shows the conic markings on the two matching fracture surfaces of PES fractured in different modes. PES experiences little plastic deformation during brittle fracture process so that the conic markings always appear concave and convex, respectively, on the matching surfaces (Fig. 5a). While PES fractures in a ductile mode, more plastic deformation happens and area of concave zone in conic markings is larger (Fig. 5b). The brittle–ductile transition of polymers can be analyzed by comparing the matching morphology of conic markings.

Simulation of conic markings

The type I conic marking is attributed to the interaction of a straightly fronted main crack O_1 with a radial growing secondary crack O_2 while the type II conic marking results from the interaction of the secondary crack O_2 with another

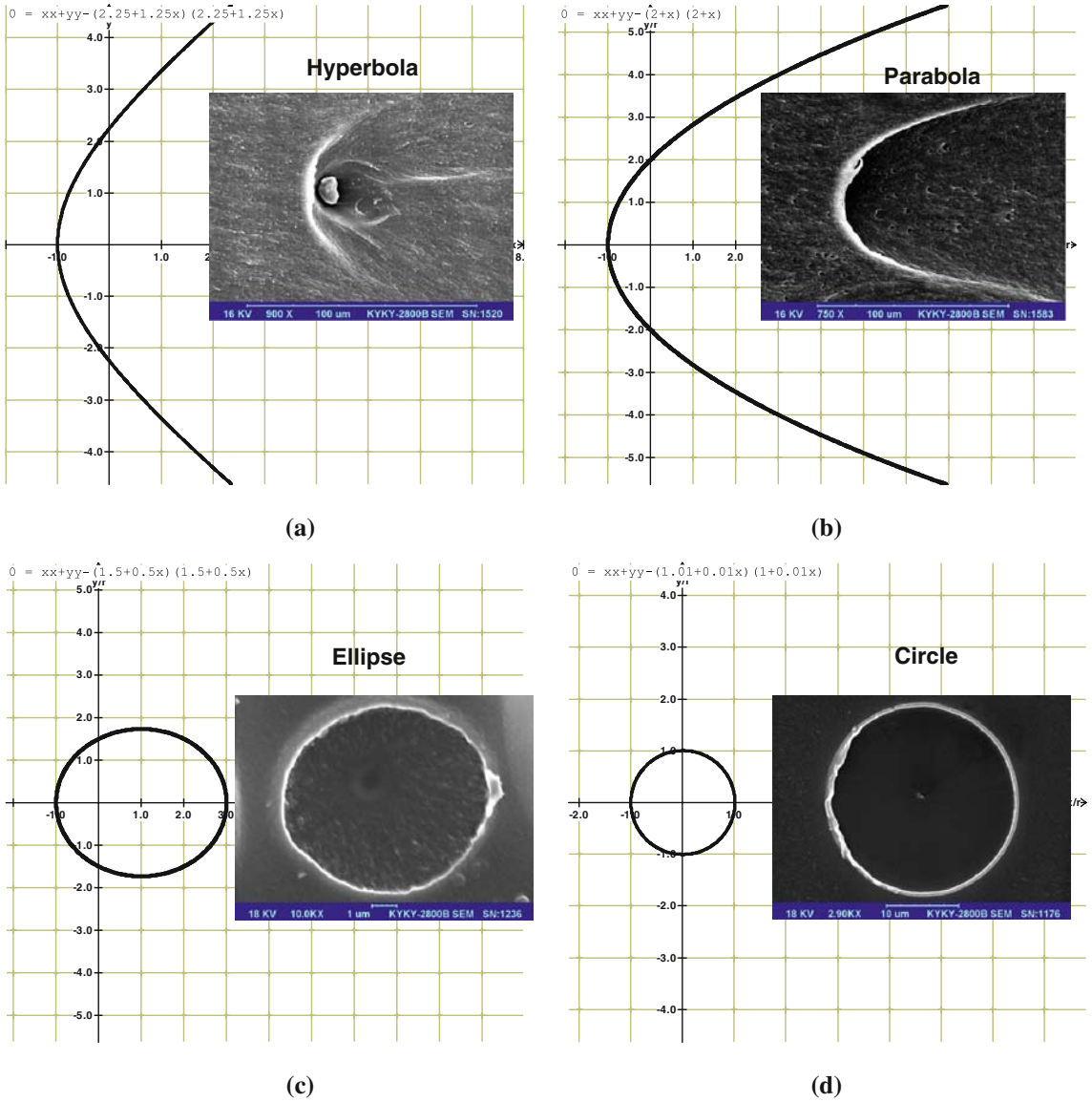

Fig. 7 Simulated conics for $V_m/V_s = 0.8$ (**a**), 1.0 (**b**), 2.0 (**c**), and 10 (**d**). The simulated conics could account for the observed hyperbola on the bending fracture surface of PPS tested at 0.05 mm/min (**a**), parabola on the bending fracture surface of PPS tested at 500 mm/min (**b**), ellipse on the impact fracture surface of PES tested at −20 °C (**c**), and circle marking on the impact fracture surface of PES tested at 60 °C (**d**)

radial growing secondary crack O_3 [41–44]. Figure 6 sketches the cracks and the conic markings in reference to a system of coordinates with the origin located at the initiation site of the first secondary crack O_2 and the x-axis parallel to the main crack growth direction. The radius of the first secondary crack O_2 is assumed to reach r at time t_1 when the main crack front first meets the front of O_2. The interaction of the front of the main crack O_1 with that of the secondary crack O_2 yields type I conic markings denoted as curves a, b, c, and d. As the cracks propagate, the front of O_2 after advancing a distance S_1 at time t_2 meets that of O_3 that advances a distance S_2. Their interaction results in the type II conic markings denoted as curves e and f.

The type I conic marking

Assuming that the main crack propagates right with a velocity of V_m and all the secondary cracks grow radially at a speed V_s [14], the equations of motion of the main and the secondary cracks can be written as, respectively,

$$X = -r + V_m t_1 \tag{1}$$

$$X^2 + Y^2 = (r + V_s t_1)^2 \tag{2}$$

A combination of Eqs. 1 and 2 yields a control equation

$$\left(\frac{X}{r}\right)^2 + \left(\frac{Y}{r}\right)^2 = \left(1 + \frac{V_s}{V_m} + \frac{V_s X}{V_m r}\right)^2 \tag{3}$$

for the intersection loci of the moving planar main crack O_1 and the secondary crack O_2. Equation 3 suggests that the specific shape of the type I conic marking depends on the ratio of the main crack velocity to the secondary crack velocity, V_m/V_s. For $V_m/V_s \approx 0$, the conic marking approximates a straight line. For $0 < V_m/V_s < 1$, the conic marking is a hyperbola with eccentricity and opening decreasing with increasing V_m/V_s and the marking becomes parabolic at $V_m/V_s = 1$. The marking appears as ellipse with eccentricity decreasing with increasing V_m/V_s above 1 and contracts into circle at V_m/V_s approaching infinite.

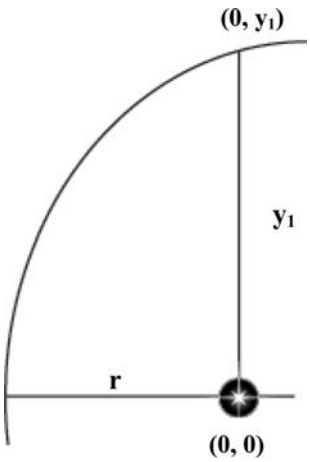

Fig. 8 Schematic diagram for measuring r and y_1

The fracture surface patterns were simulated using a mathematical software "*winplot*" (Peanut Software Co.). Figure 7 shows the simulated conics at different V_m/V_s, which could well account for the typical SEM micrographs observed on the fracture surfaces.

By measuring r and y_1 (Fig. 8) and substituting into Eq. 3, conic markings can be used to analyze the crack growth velocity through:

$$V_m/V_s = r/(y_1 - r). \tag{4}$$

Figure 9 presents variation of the conic shapes with the crack propagation observed on tensile fracture surface of PEI and bending fracture surface of PPS. The hyperbola or parabola markings in the initiation change to ellipses or

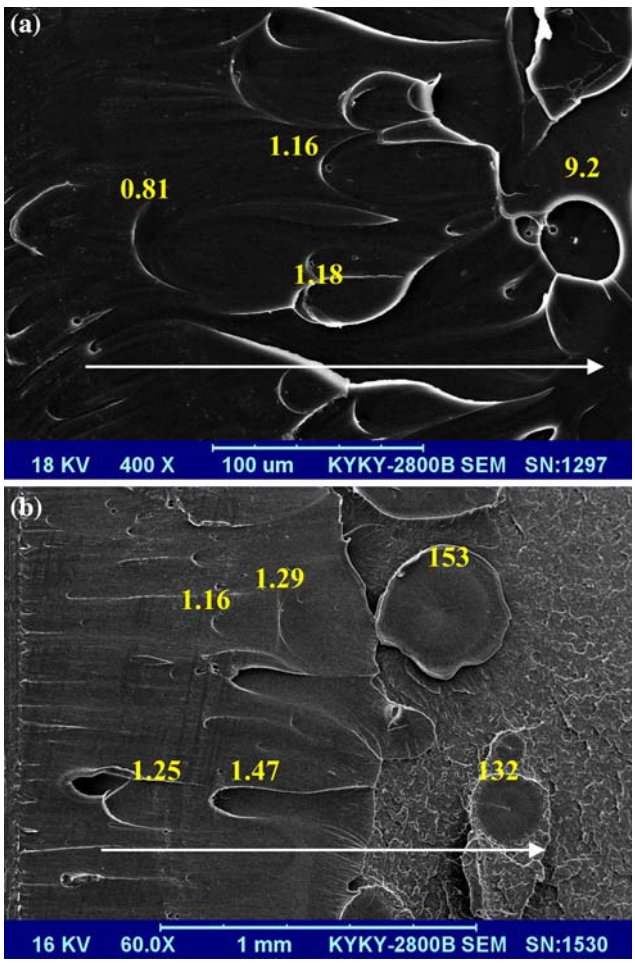

Fig. 9 SEM micrographs showing the variation of conics and the corresponding V_m/V_s values along with the crack propagation on the tensile fracture surface of PEI tested at 100 mm/min (**a**) and the bending fracture surface of PPS tested at 190 mm/min (**b**). The *white arrows* denote the direction of crack propagation

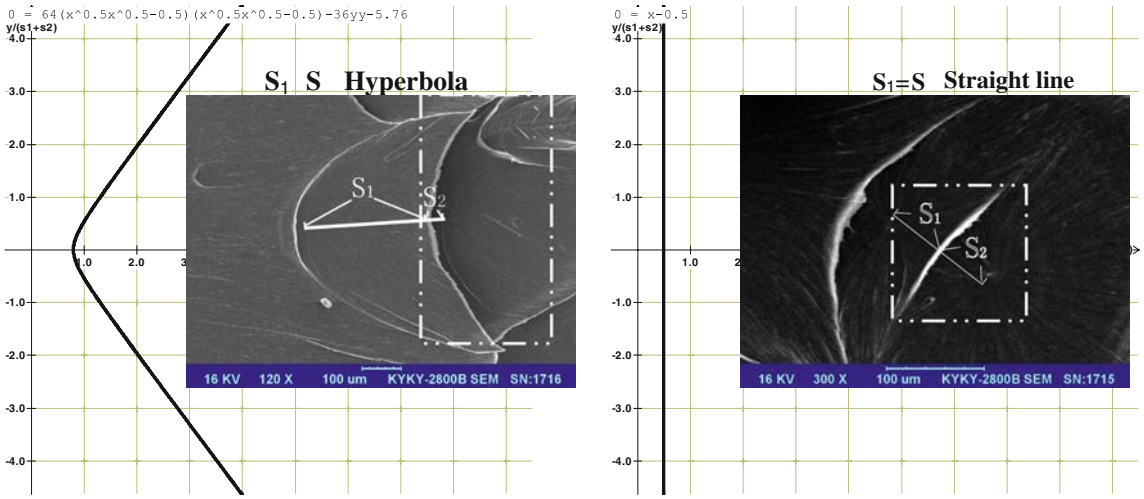

Fig. 10 Simulated hyperbola conic for $S_1 \neq S_2$ (**a**) and straight line conic for $S_1 = S_2$ (**b**). SEM micrographs on tensile fracture surfaces of PES tested at 500 mm/min (**a**) and PES tested at 500 mm/min (**b**) are shown

circles with the crack propagation and the values of V_m/V_s are also labeled near the corresponding conic markings. V_m/V_s increases gradually along with the crack propagation.

The fracture surfaces can be classified as fracture initiation zone, fracture spreading zone, and transient breaking zone. Under external stress, the crack growth velocity continues to increase gradually from zero to relatively high values as the main crack departs from the initiation zone [14] so that V_m/V_s increases gradually along with the crack propagation. Such variations of the conic shapes and V_m/V_s are in good agreement with fracture process, so variations of conic shapes can help to determine the crack growth velocity more accurately.

The type II conic marking

The equations of motion of the secondary cracks O_2 and O_3 are given by

$$X^2 + Y^2 = (S_1 + V_s t_2)^2 \tag{5}$$

$$(X - S_1 - S_2)^2 + Y^2 = (S_2 + V_s t_2)^2 \tag{6}$$

A combination of Eqs. 5 and 6 yields a control equation

$$4S_1S_2(X - S_1/2 - S_2/2)^2 - (S_1 - S_2)^2 Y^2 = S_1S_2(S_1 - S_2)^2 \tag{7}$$

for the intersection loci of the two secondary cracks O_2 and O_3. Equation 7 reveals that the specific shape of the type II conic marking depends on the distances that two secondary cracks have propagated before they meet, S_1 and S_2. When $S_1 = S_2$, the interaction shape is a straight line and otherwise, the interaction shape is a hyperbola. Figure 10 shows the simulated results for $S_1 \neq S_2$ and $S_1 = S_2$, respectively, which could well account for the typical SEM micrographs observed on the fracture surfaces.

Conclusions

The inhomogeneities that trigger the initiation of secondary cracks may be impurities, microvoids, discontinuities in preferred orientation/birefringence, residual stresses, and type and characteristics of morphological zones in case of semicrystalline polymers. Most conic shapes exhibit stepped morphology in stereo configuration, and the secondary crack origin is depressed in the plane of secondary crack as a result of plastic deformation. The brittle–ductile transition of polymers can be analyzed by comparing the matching morphology of conic markings. Computer simulations demonstrate that the shape of type I conic markings is determined by the ratio of main crack velocity to secondary crack velocity, V_m/V_s. The type I conic marking changes from a hyperbola to a parabola, an ellipse and finally to an approximating circle with increasing V_m/V_s. The shape of the type II conic markings depends on the two distances S_1 and S_2 that two secondary cracks have covered before they meet. The interactions are a straight line when $S_1 \neq S_2$ or a hyperbola when $S_1 = S_2$. Variations of conic shapes are helpful for determining the change of crack growth velocity.

Acknowledgements The authors gratefully acknowledge the financial support for this work from Guizhou Flare Plan (No. 20008005) and Guizhou Science Fund (No. 20003072).

References

1. Kies JA, Sullivan AM, Irwin GR (1950) J Appl Polym Sci 21:716
2. Yuan Q, Misra RDK (2006) Polymer 47:4421
3. Doyle MJ (1982) J Mater Sci 17:760. doi:10.1007/BF00540373
4. Luo WB, Yang TQ, Wang XY (2004) Polymer 45:3519
5. Cheng CM, Hiltner A, Baer E, Soskey PR, Mylonakis SG (1994) J Appl Polym Sci 52:177
6. Liu K, Piggott MR (1998) Polym Eng Sci 38:60
7. Mathew AP, Thomas S (2001) Mater Lett 50:154
8. Wu HY, Ma G, Xia YM (2004) Mater Lett 58:3681
9. Lee EKC, Rudin A, Plumtree AJ (1995) J Mater Sci 30:2091. doi:10.1007/BF00353039
10. Kulawansa DM, Langford SC, Dickinson JT (1992) J Mater Res 7:1292
11. Zhang MJ, Zhi FX, Su XR (1989) Polym Eng Sci 29:1142
12. Luo WB, Yang TQ (2003) J Appl Polym Sci 89:1722
13. Matsushige K, Sakurada Y, Takahashi K (1984) J Mater Sci 19:1548. doi:10.1007/BF00563052
14. Ravichandar K, Yang B (1997) J Mech Phys Solids 45:535
15. Doyle MJ (1983) J Mater Sci 18:687. doi:10.1007/BF00745566
16. Lednicky F (1984) Polym Bull 11:579
17. Lin YC, Chen X (2005) Mater Lett 59:3831
18. Matsuda T, Tai K (1997) Polymer 38:1669
19. Takenaka M, Nishitsuji S, Taniguchi T, Yamaguchi M, Tada K, Hashimoto T (2006) Polymer 47:7846
20. Melker AI, Ivanov AV (1984) Phys Status Solidi A 84:417
21. Oshmyan VG, Shamaev MY, Timan SA (2003) J Appl Polym Sci 89:2771
22. Rabinovitch A, Belizovsky G, Bahat D (1993) Int J Fract 63:25
23. Rozanski A, Monasse B, Szkudlarek E, Pawlak A, Piorkowska E, Galeski A, Haudin JM (2009) Eur Polym J 45:88
24. Mago G, Fisher FT, Kalyon DM (2008) Macromolecules 41:8103
25. Zhang RC, Xu Y, Lu A, Cheng KM, Huang YG, Li ZM (2008) Polymer 49:2604
26. Su R, Wang K, Zhao P, Zhang Q, Du RN, Fu Q, Li LB, Li L (2007) Polymer 48:4529
27. Zhang WD, Martins JA (2007) Polymer 48:6215
28. Zhang CG, Hu HQ, Wang DJ, Yan S, Han CC (2005) Polymer 46:8157
29. TT Wang (1973) J Appl Phys 44:2218
30. Wang TT (1973) J Appl Phys 44:4052
31. Wang TT (1974) J Polym Sci Pol Phys 12:145
32. Wang TT (1992) Macromolecules 25:933
33. Van Dommelen JAW, Parks DM, Boyce MC, Brekelmans WAM, Baaijens FPT (2003) Polymer 44:6089
34. Nitta KH, Takayanagi M (2003) J Mater Sci 38:4889. doi:10.1023/B:JMSC.0000004410.56145.f1
35. Wagner A, Yu J, Kalyon DM (1989) Polym Eng Sci 29:1298
36. Yu J, Wagner AH, Kalyon DM (1992) J Appl Polym Sci 44:477
37. Yu J, Kalyon DM (1991) Polym Eng Sci 31:153
38. Yu J, Lim M, Kalyon DM (1991) Polym Eng Sci 31:145
39. Wagner A, Yu J, Kalyon DM (1989) Adv Polym Tech 9:17
40. Wagner A, Kalyon DM (1991) Polym Eng Sci 21:1393
41. Sharon E, Cohen G, Fineberg J (2002) Phys Rev Lett 88:1
42. Morrissey JW, Rice JR (1998) J Mech Phys Solids 46:467
43. Fineberg J, Sharon E, Cohen G (2003) Int J Fract 121:55
44. Morrissey JW, Rice JR (2000) J Mech Phys Solids 48:1229